

Influence of the backward-pump process on photon-number squeezing in a constant-current-driven heterojunction LED: Transition from thermionic emission to diffusion limits

Masahide Kobayashi, Masamichi Yamanishi,* Hiroyuki Sumitomo, and Yutaka Kadoya

Department of Physical Electronics, Faculty of Engineering, and Hiroshima-Branch of Research Projects for Core Research for Evolutional Science and Technology (CREST), JST, Hiroshima University, 1-4-1 Kagamiyama, Higashi-Hiroshima 739-8527, Japan

(Received 30 April 1999)

Physical mechanisms which limit the squeezing bandwidth in a heterojunction light-emitting diode (LED) have been extensively studied both theoretically and experimentally. It is proven that our experimental results of pump-current dependence of the squeezing bandwidth in the constant-current-driven heterojunction LED at room temperature cannot be explained by previous theoretical predictions. We present a theoretical framework, including the effects of a microscopic backward-pump (BP) process, generally applicable to a heterojunction LED. Parameters describing the relative significance of the BP process are determined by the measurements of current-versus-voltage characteristic and differential resistance of the LED, independent of the noise measurements. As a consequence, the experimental results can be explained by our model in a unified manner over a whole range of injection current, and it is clarified that the pump situation of the LED moves continuously from thermionic emission to diffusion limits with increasing pump current. [S0163-1829(99)09247-4]

I. INTRODUCTION

Generation of nonclassical lights, such as photon-number squeezed states and quadrature-phase squeezed states, is expected to conquer the difficulties due to the standard quantum limit (SQL) of classical (coherent) lights, in a variety of applications ranging from optical communications to biology where the capacity of light to carry information is limited by photon-number fluctuations. A photon-number squeezed state, having photon-number uncertainty Δn smaller than that of coherent lights (the square root of the average number, $\sqrt{n_0}$ of Poissonian distribution), is termed a sub-Poissonian photon state. Among a variety of schemes, direct generation of sub-Poissonian photon fluxes from semiconductor light emitters has been attracting much attention since the first theoretical prediction¹ and successive experimental works,^{2,3} because of the simplicity of experimental arrangement, the low-energy consumption, the possibility of a large degree of noise suppression, and the compatibility to modern communication systems. So far, the reduction of photon-number noise below the SQL level has been observed using semiconductor laser diodes (LDs) (Refs. 2 and 4) or light-emitting diodes (LEDs) (Refs. 3 and 5–10) driven by high-impedance constant-current sources and series coupled LEDs driven by constant-voltage sources.^{11,12} The quantum correlated twin beams have been predicted¹³ and observed with coupled LEDs (Refs. 11, 12, and 14) and LDs.¹⁵ In an engineering view, such as device uses in few photon direct-detection optical communication systems, the LED (spontaneous-emission) mode operation is of crucial importance since LEDs can have higher quantum efficiencies at very low current regime, and as a result, weak sub-Poissonian fluxes can be generated with LEDs even at pump rates far below the threshold for the onset of lasing.¹⁶

In the case of constant-current driving of an LED or LD,

the current shot noise of a resistor in source circuit can be suppressed by inelastic electron scatterings.^{17–19} However, the suppression of current noise does not necessarily guarantee the suppression of shot noise in output photon fluxes in semiconductor light emitters, since the dynamics of pump and recombination processes could also affect the squeezing.^{1,20,21} Recently, Kim *et al.* have analyzed the influence of carrier flow (pump process) across the depletion layer of a p - n junction on the squeezing of output photon-number fluctuations.²² They took account of both microscopic stochastic forward- (FP) and backward-pump (BP) events on the basis of a macroscopic diffusion model for the carrier transport in a p - n homojunction, and obtained an analytical expression for the squeezing bandwidth in terms of the time constants of pump and recombination processes. On the other hand, prior to the diffusion model, a thermionic-emission model has been proposed by Imamoglu *et al.* for a hetero p - n junction LED, where they ignored the BP process, and analyzed the squeezing bandwidth governed by the forward thermionic-emission process under the assumption that the recombination events take place immediately after the electron pump events.^{23,24} Recently, we have demonstrated the squeezing over a wide frequency range reaching 100 MHz at room temperature using commercially available high-performance (high-speed and high-quantum-efficiency) heterojunction LEDs.¹⁰ The widest 3-dB squeezing bandwidth of ~ 60 MHz obtained at high injection currents is basically limited by the recombination dynamics of electrons, while the bandwidth at the low injection current regime is done by the time constant of “macroscopic Coulomb blockade”^{6,9} for the pump process. However, the observed current dependence of the bandwidth in the intermediate current regime can be fitted by neither the diffusion²² nor thermionic model.²⁴

In addition to the high impedance noise suppression, a

new scheme termed the quantum-confined Stark effect (QCSE) blockade¹⁶ has been proposed, which allows us the direct regulation of emission events and, as a result, in which the high-impedance circuit is not necessarily required for the squeezing. Such a new understanding of the emission process may open up a new opportunity in future applications of sub-Poissonian photon states.

In the present work, we study in detail physical mechanisms which limit the squeezing bandwidth in the heterojunction LED driven by a constant-current source at room temperature. It is shown that in the LED operating in the intermediate current regime, the BP rate relative to the FP rate increases substantially as the injection current increases, and the experimental results of the squeezing bandwidth can be explained in a unified manner over a whole range of injection currents in terms of our model proposed in this paper. In Sec. II, we will briefly review the previous predictions for the squeezing bandwidth in constant-current-driven LEDs. Then, our experimental results of photon-number squeezing obtained with the high-speed heterojunction LED driven by a constant-current source will be presented in Sec. III. In Sec. IV A, we will present our theory, which, without the assumption of any specific models for the BP process, includes phenomenological parameters to represent the influence of the BP process, and in Sec. IV B, the experimental procedures to determine the parameters will be shown. Then in Sec. IV C, we will show that the experimental results of the squeezing bandwidth are successfully interpreted in terms of our theoretical model. In Sec. V, we will give some conclusions.

II. BRIEF REVIEW OF THE THEORY OF SQUEEZING BANDWIDTH

Here, we briefly review theoretical models proposed so far for the interpretation of physics behind sub-Poissonian photon generation in LEDs driven by high-impedance constant-current sources. The current source noise described by Johnson-Nyquist noise in a resistor, R_s , can be much weaker than the full shot noise of a current flow, i.e., $4k_B T/R_s \ll 2eI_{\text{LED}}$ if R_s is sufficiently high, where k_B , T , e , and I_{LED} are the Boltzmann constant, the device temperature, the elementary charge, and the dc pump current of an LED, respectively. However, “quiet electron flows” created by high-impedance constant-current sources do not necessarily lead to the generation of “quiet photon flows.”^{1,20} Figure 1 shows the energy band diagram of a hetero- p - n junction LED. The conduction electrons have to be supplied to a p -doped active region from an n -doped wide-band-gap region across the potential barrier by thermionic emission, diffusion, or tunneling processes. Such an electron transport process is a completely random point (stochastic) one on a microscopic level as it is caused by the collision of electrons with phonons. Hence, “quiet electron flows” are disturbed, and the extra noise would be added to the carrier injection process. Fortunately, however, the macroscopic pump rate is regulated even in the conventional macrosized LEDs or LDs through a negative feedback mechanism owing to the junction voltage fluctuations induced by the resultant effects of many pump events, if the time window (measurement time) Δt is much wider than the thermionic-emission time $\tau_{\text{te}} = k_B T C_{\text{dep}} / (eI_{\text{LED}})$, where C_{dep}

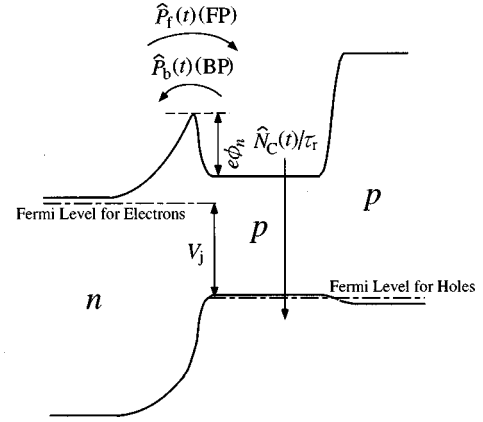


FIG. 1. Typical energy-band diagram under the forward-bias condition of a commercial p - n heterojunction light-emitting diode (LED). Band-gap gradings at the interfaces between the n -type wide gap and active regions and between the active and p -type wide gap regions are taken into account (for a detailed discussion on potential profiles in a graded-gap junction diode, see Appendix B).

is the junction capacitance.^{1,6,24} Namely, the regulation bandwidth for the pump process is given by $1/(2\pi\tau_{\text{te}})$. This regulation mechanism is sometimes termed “macroscopic Coulomb blockade” or “collective Coulomb blockade.”^{6,22,24} It is interesting to note that the inequality to realize the source-noise suppression, $4k_B T/R_s \ll 2eI_{\text{LED}}$, is equivalent to the condition, namely $R_s \gg$ differential resistance of LED, $r_d \cong k_B T / (eI_{\text{LED}})$, under which the junction voltage can fluctuate freely and the pump current is kept constant despite the junction voltage fluctuations. In addition to the normal injection of electrons (FP) considered above, the reverse current flow, i.e., the backward transport of conduction electrons from the p -type active to the n -type wide-band-gap regions (BP), may exist on a microscopic level. The (net) average current is given by the difference between the FP and BP rates. In the noise analysis, each process has to be treated separately. The way to treat the BP process has not yet been well-established and is a key issue of the present work.

Another random point process is involved in the radiative recombination process of injected carriers. Spontaneous decay of the excited electrons has a shot-noise character because vacuum-field fluctuations (VFFs) trigger spontaneous emissions. However, the free fluctuations of the electron population N_C in the active region induced by the random emission events bring us an internal negative feedback for the emission events. Namely, the fluctuations of the photon emission rate associated with the population fluctuations cancel the shot noise originally involved in the photon emission process, as far as the measurement time window is wider than the recombination lifetime of the carriers, τ_r , the time required for an appreciable change in the electron population. Thus, the bandwidth for the regulation of the emission process due to the fluctuations of electron population is given by $1/(2\pi\tau_r)$.

It may be naturally predicted that the squeezing bandwidth of photon-number fluctuations is characterized by both the characteristic time constants of the pump and recombination dynamics. In fact, adopting the macroscopic diffusion model to an LED, Kim *et al.*²² have obtained an expression for the squeezing bandwidth (3-dB rolloff bandwidth) f_c as

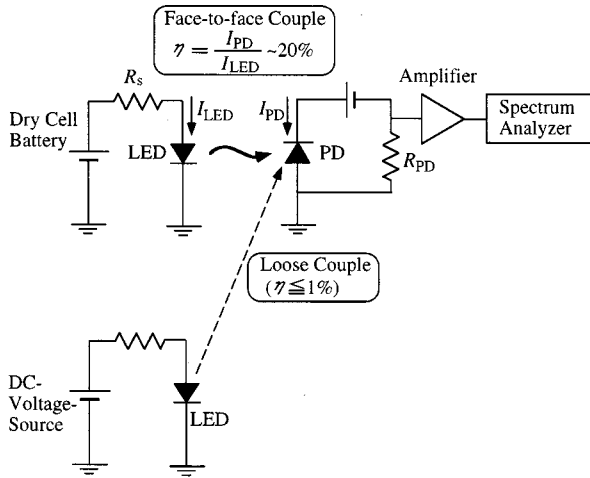


FIG. 2. Schematic diagram of the experimental arrangement. For the measurement of sub-Poissonian photon state, the light-emitting diode (LED) was coupled tightly to the photodiode (PD). On the other hand, in order to calibrate the full shot-noise (FSN) level, another LED was coupled weakly to the PD.

$$f_c = \frac{1}{2\pi(\tau_{te} + \tau_r)} = \frac{1}{2\pi\left(\frac{k_B T C_{dep}}{e I_{LED}} + \tau_r\right)}. \quad (1)$$

Some experimental results have been fitted rather well by Eq. (1).^{6,9} However, it is questionable whether the macroscopic diffusion model is applicable generally to heterojunction LEDs, since the BP rate is to strongly depend on the band-gap discontinuities in the heterostructure devices. Indeed, our experimental results cannot be interpreted in terms of the theoretical curve estimated with Eq. (1), as will be shown later. On the other hand, Imamoglu *et al.*²⁴ focused on another extreme case where carrier injection into the active region is caused only by the thermionic- (forward-) emission process in a heterojunction LED. Under the assumption that the injected carriers recombine instantaneously, they showed that the squeezing bandwidth is given by $f_c = e I_{LED} / (2\pi k_B T C_{dep})$. However, such assumption may not again be valid for our LED where the BP process takes place more or less particularly at room temperature.

III. NOISE MEASUREMENTS

A. Experimental arrangement

A schematic diagram of the experimental arrangement for room-temperature measurements is shown in Fig. 2. A high-speed $\text{Al}_x\text{Ga}_{1-x}\text{As}$ LED (Hitachi HE8812SG), whose emitting surface is shaped hemispherically to give rise to a high external quantum efficiency,²⁵ has a double heterojunction (DH) structure, $n\text{-Al}_{0.2}\text{Ga}_{0.8}\text{As}/0.5\text{-}\mu\text{m-thick } p\text{-Al}_{0.01}\text{Ga}_{0.99}\text{As}/p\text{-Al}_{0.2}\text{Ga}_{0.8}\text{As}$ and an emission spectrum, $\lambda \sim 860$ nm, peaking in the high sensitivity wavelength range of a high quantum efficiency silicon $p\text{-}i\text{-}n$ photodiode (PD) (Hamamatsu S6040). The LED was connected to a voltage source (a dry cell battery) through a metal-film resistor $R_s = 2$ K Ω , much higher than the differential resistance r_d of the LED ($R_s \gg r_d$), i.e., the LED was driven by a high-impedance constant-current source. For the measurement of

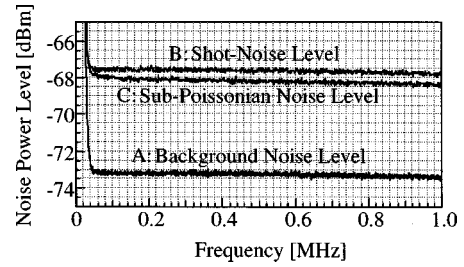


FIG. 3. Typical traces of spectral photocurrent noise detected by the photodiode (PD). Bottom trace A is the background noise obtained without illumination for the PD, top trace B is the photocurrent noise obtained with the PD coupled weakly to a light-emitting diode (LED), and middle trace C is the photocurrent noise obtained with the test LED driven with a constant-current source. The data were obtained with a resolution bandwidth of 10 KHz, a video bandwidth of 30 Hz, and a sweep time of 10.24 s.

sub-Poissonian photon states, the LED was placed just in front of the PD to yield a high current-to-current conversion efficiency (photodetector current, $I_{PD}/\text{LED-pump-current}$, I_{LED}), $\eta \sim 20\%$ at room temperature.¹⁰ The output current flow in the PD was converted to a voltage signal through a load resistor ($R_{PD} = 330$ Ω). Then, the noise signal was amplified by an ultralow noise preamplifier (NF SA-220F5) and was finally fed to a spectrum analyzer (HP HP4396A). The high-frequency characteristic of the detection system was primarily limited by that of the RC low-pass circuit formed by the capacitance of the PD, the input capacitance of the preamplifier, and the load resistor.

To determine experimentally the full shot-noise (FSN) level (reference level), the PD was illuminated by another LED (HE8812SG) located far away from the PD to reduce the coupling efficiency, $\eta \leq 1\%$.¹⁰ We can compare directly the measured FSN level with the theoretical prediction $2eI_{PD}$ in the low-frequency range, $f \leq 1$ MHz, where the circuit voltage gain of the detection system is identified to be a certain value, 200. Figure 3 shows typical traces of the noise levels on the spectrum analyzer focused on the low-frequency regime $f \leq 1$ MHz. Trace A obtained without illumination for the PD is the background noise level consisting of thermal noise of the load resistor and amplifier noise, trace B obtained by illuminating the PD in the low coupling arrangement represents the sum of FSN level and background noise level, and trace C obtained by driving the test LED adjacent to the PD does the sum of sub-Poissonian photon noise level and background noise level. The experimental value of the FSN level (trace B minus trace A) at the frequency range 50 KHz $\leq f \leq 1$ MHz was confirmed to be in very good agreement with the theoretical one, $2eI_{PD}$, within a very small error of $\sim 0.2\%$. The normalized spectral noise power density of sub-Poissonian photon fluxes is evaluated from these traces as $(\text{trace C} - \text{trace A}) / (\text{trace B} - \text{trace A})$. The obtained normalized spectral density is equal to the spectral Fano factor defined as the ratio of spectral noise power density to dc quantity, $(\delta I_{PD}/e)^2 / (I_{PD}/e)$, because of $(\delta I_{PD}/e)^2 = I_{PD}/e$ for the shot-noise case, where $(\delta I_{PD})^2$ is the spectral noise power per unit frequency band in the detector current. Since the circuit geometry of the detection system is fixed in these measurements, we can obtain the Fano factor over a wide

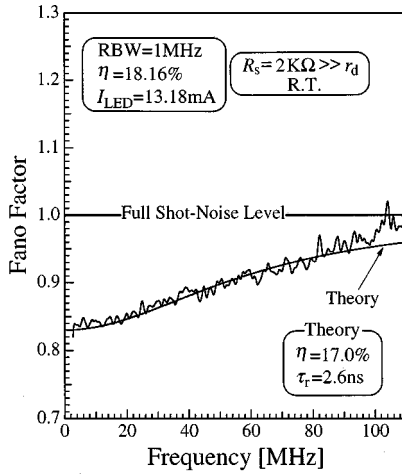


FIG. 4. Spectral Fano factor of output photon fluxes over a wider frequency range obtained with a high-speed light-emitting diode (LED) (Hitachi HE8812SG) driven by a constant-current (13.18 mA) source at room temperature. The data were obtained with a resolution bandwidth of 1 MHz, a video bandwidth of 3 KHz, and a sweep time of 5.12 s. For a comparison with the experimental result, the theoretical curve estimated with Eq. (2) is also indicated. The values of overall quantum efficiency and recombination lifetime are used, in the estimation, to be $\eta=0.17$ and $\tau_r=2.6$ ns, respectively.

frequency range without corrections associated with the frequency characteristic of the detection circuit as far as the circuit gain is high enough to discriminate the signal on the spectrum analyzer from the background noise level. The whole measurement system was installed inside a shield room.

B. Wide-band squeezing of photon-number fluctuations

Figure 4 shows the spectral Fano factor of detected photons, $F_d(f)$, for a LED-pump current of 13.18 mA and a quantum efficiency of $\eta=18.16\%$, demonstrating a substantial noise suppression below the FSN level over a wide frequency range from near dc to 100 MHz.¹⁰ In this relatively high current regime, thermionic response time of the p - n junction is much shorter than the recombination lifetime in the active layer, $\tau_r=2.6$ ns \gg $\tau_{te}=k_B T C_{dep}/(eI_{LED})=0.14$ ns with $C_{dep}=70$ pF, and the squeezing bandwidth is primarily limited by the recombination dynamics. By fitting of the experimental result with the theoretical curve for such a case,²⁶

$$F_d(f) = 1 - \eta + \eta \frac{(2\pi f \tau_r)^2}{1 + (2\pi f \tau_r)^2}, \quad (2)$$

we obtain $\eta=0.17$, which is reasonably close to the experimental value obtained with dc measurement ($\eta=0.1816$) and $\tau_r=2.6$ ns, also close to the widely accepted value, $\tau_r \sim 3$ ns,²⁷ of the electron lifetime in a highly p -doped ($\sim 10^{18}$ cm⁻³) GaAs, which is the active layer material (though more strictly, Al_{0.01}Ga_{0.99}As) of the present LED. The short recombination lifetime of electrons enabled us to observe the wide-band squeezing of photon-number fluctuations. The bandwidth of the noise suppression, f_c , defined as the frequency at which the degree of noise reduction is half

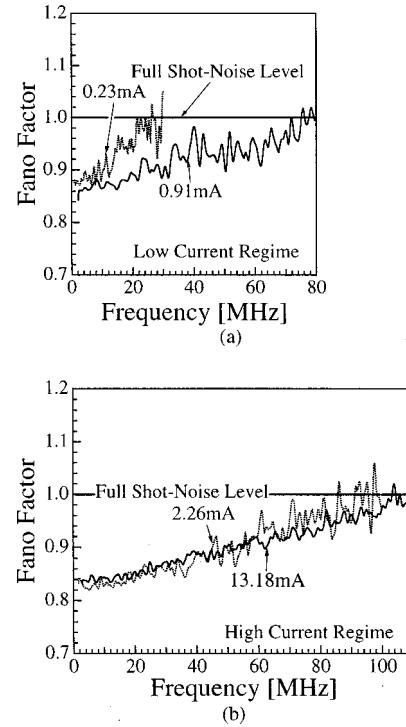


FIG. 5. Spectral Fano factors of output photon fluxes from the same light-emitting diode (LED) as in Fig. 4 obtained with four different pump currents [(a) 0.23 mA and 0.91 mA and (b) 2.26 mA and 13.18 mA]. The data for $I_{LED}=0.23$ mA were obtained with a resolution bandwidth of 300 KHz, a video bandwidth of 1 KHz, and a sweep time of 5.12 s, and the data for the other currents were obtained with the same condition as in Fig. 4.

the maximum suppression at the low-frequency limit, is observed to be ~ 60 MHz in this specific case, which is the widest ever reported with LEDs. This bandwidth for the noise suppression is very close to 3-dB bandwidth of optical output for external current modulation of the same type LED as ours, reported in Ref. 25.

Figures 5(a) and 5(b) show the spectral Fano factors of photon number detected by the PD for four different LED-pump currents (0.23 mA, 0.91 mA, 2.26 mA, and 13.18 mA). In the low current regime [Fig. 5(a)], the squeezing bandwidth is obviously expanded with the increase of pump current, whereas in the high current regime [Fig. 5(b)] the squeezing bandwidth is almost unchanged. In the next subsection, the pump-current dependence of the squeezing bandwidth will be demonstrated to investigate the squeezing mechanism of photon-number fluctuations in the heterojunction LED.

C. Pump-current dependence of the squeezing bandwidth

As a result of the careful measurements carried out with the high-performance LED, we obtained precisely systematic experimental results on the current dependence of the squeezing bandwidth, which may allow a qualitative discussion on the physical mechanisms which limit the squeezing bandwidths at various injection current levels. The measured squeezing bandwidths (squares) at room temperature are plotted as a function of pump-current I_{LED} (or corresponding current density) in Fig. 6. In the measurements, the resis-

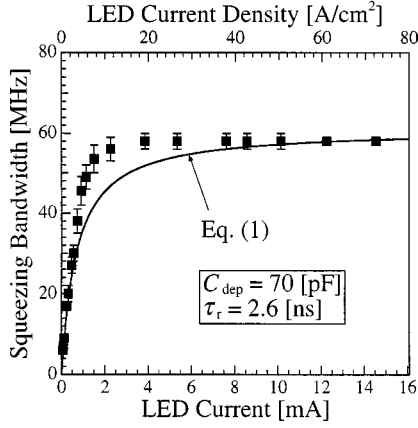


FIG. 6. Measured pump-current (-density) dependence of the squeezing bandwidth of the high-speed light-emitting diode (LED) driven by constant-current sources at room temperature. The experimental results are compared with the theoretical curve estimated with Eq. (1), using $C_{\text{dep}}=70$ pF and $\tau_r=2.6$ ns.

tance $R_s=2$ K Ω , through which the LED was driven, was chosen to meet the constant-current condition ($R_s \gg r_d$) for all the current levels. The solid curve shows the theoretical prediction estimated with Eq. (1). In the estimation, the junction capacitance $C_{\text{dep}}=70$ pF and the reasonable recombination lifetime $\tau_r=2.6$ ns were chosen independently so as to result in the best fittings between theory and experiments in the low and high I_{LED} limits, respectively. The postulated value $C_{\text{dep}}=70$ pF was reasonably close to the measured diode capacitance 50 pF at an applied forward voltage of 1.3 V, which is slightly lower than the bias voltages used in the noise measurements, $V=1.35\text{--}1.5$ V. Nevertheless, the experimental values obviously deviate from the theoretical ones in the mid- I_{LED} range, $I_{\text{LED}}=0.6\text{--}10$ mA indicating that Eq. (1) cannot be used to explain the experimental results over the whole range of I_{LED} . In other words, the macroscopic diffusion model is not applicable to the present heterojunction LED unlike a homojunction LED.²² In the next section, we will propose a model which will eventually interpret our experimental results over the entire range of I_{LED} .

IV. UNIFIED MODEL FOR THE SQUEEZING BANDWIDTH

A. Framework of the backward-pump model

Let us go back to the energy-band diagram of a heterojunction LED under a forward-bias condition shown in Fig. 1. The LED (HE8812SG) used in the present work would be viewed electrically as a single p - n -junction device since the active and p -type wide-band-gap regions of the LED are highly p -doped,²⁵ $N_a > 1 \times 10^{18}$ cm⁻³, much higher than the doping concentration in the n -type wide-band-gap region, $N_d \sim 1 \times 10^{17}$ cm⁻³, as will be discussed in Appendix B. In other words, the voltage drops across the p -type active region and the p - p heterojunction between the active and p -type wide-band-gap regions are negligibly low compared with the voltage drop across the p - n junction. The device performance of such a LED may be characterized by electron transport from the n -type wide band gap to p -type active

regions and by recombination dynamics of electrons in the active region. The injected electron density in the active region is estimated to be 5×10^{16} cm⁻³ even with the highest LED current, 20 mA used in the present work, which is much lower than the doped hole concentration ($> 10^{18}$ cm⁻³) in the active region. This may justify the use of a linear recombination model. Another important point to be considered is backward electron transport, which is termed the backward-pump (BP) process in this paper, from the active to n -type wide-band-gap regions. In general, the excess energy of an electron thermally injected from the n -type region into the p -type active region is relaxed quickly by its interaction with phonons, other electrons, and holes. However, for a high pump current, some of the injected electrons may no longer be completely relaxed down to around the conduction-band edge because of the hot carrier effect²⁸ and/or band filling. As a result, electrons with energies higher than the n -side barrier height, $e\phi_n$, of the heterojunction can go back the n -type layer and thus the BP process may take place as shown in Fig. 1. Hence, the LED should be viewed as a quantum-mechanical system including such a BP process.

We start by putting the operators, written in the Heisenberg picture, representing the electron FP rate, $\hat{P}_f(t)$, the electron BP rate, $\hat{P}_b(t)$, and the emission (electron linear recombination) rate, $\hat{N}_C(t)/\tau_r$, in the active region with the electron population $\hat{N}_C(t)$ and the photon flux $\hat{\Phi}(t)$ detected by a PD with an efficiency η , as the sums of their steady-state (average) and small fluctuation terms. The corresponding Langevin noise source operators $\hat{\Gamma}_{\text{pf}}(t)$, $\hat{\Gamma}_{\text{pb}}(t)$, and $\hat{\Gamma}_{\text{sp}}(t)$ are added to the FP, BP, and emission rate operators, respectively, and $\hat{F}(t)$ is involved in the photon flux operator, to represent a complete set of time evolution of these quantities,

$$\hat{P}_f(t) + \hat{\Gamma}_{\text{pf}}(t) = P_{f0} + \Delta\hat{P}_f(t) + \hat{\Gamma}_{\text{pf}}(t), \quad (3)$$

$$\hat{P}_b(t) + \hat{\Gamma}_{\text{pb}}(t) = P_{b0} + \Delta\hat{P}_b(t) + \hat{\Gamma}_{\text{pb}}(t), \quad (4)$$

$$\frac{\hat{N}_C(t)}{\tau_r} + \hat{\Gamma}_{\text{sp}}(t) = \frac{N_{C0}}{\tau_r} + \frac{\Delta\hat{N}_C(t)}{\tau_r} + \hat{\Gamma}_{\text{sp}}(t), \quad (5)$$

$$\hat{\Phi}(t) = \Phi_0 + \Delta\hat{\Phi}(t) = \eta \frac{N_{C0}}{\tau_r} + \eta \frac{\Delta\hat{N}_C(t)}{\tau_r} + \hat{F}(t). \quad (6)$$

We define a parameter α_0 ($0 \leq \alpha_0 < 1$) as the ratio of dc BP to FP rates,

$$\alpha_0 = P_{b0}/P_{f0} = I_{b0}/I_{f0}, \quad (7)$$

where I_{f0} and I_{b0} are the average microscopic forward and backward currents, respectively. The net average current is given by $I_{\text{LED}}(\equiv I_0) = I_{f0} - I_{b0} = e(P_{f0} - P_{b0})$, and, hence, the dc values (average values) of the FP and BP rates are expressed as

$$P_{f0} = \frac{P_0}{1 - \alpha_0}, \quad (8)$$

$$P_{b0} = \frac{\alpha_0}{1 - \alpha_0} P_0 = \frac{\alpha_0}{1 - \alpha_0} \frac{N_{C0}}{\tau_r}. \quad (9)$$

The small-amplitude fluctuation $\Delta \hat{P}_b(t)$ of the BP rate can be naturally viewed as being proportional to the fluctuation of the electron population $\Delta \hat{N}_C(t)$ in the active region and being independent of the junction voltage fluctuations, $\Delta \hat{V}_j(t)$. Hence, we set

$$\Delta \hat{P}_b(t) = \frac{\alpha_d}{1 - \alpha_d} \frac{\Delta \hat{N}_C(t)}{\tau_r}, \quad (10)$$

where α_d ($0 \leq \alpha_d < 1$) would be a function of N_{C0} . Similarly, for a small shift of the dc bias point, one obtains, by using the same parameter α_d ,

$$\Delta P_{b0} = \frac{\alpha_d}{1 - \alpha_d} \frac{\Delta N_{C0}}{\tau_r}. \quad (11)$$

The parameter α_d may be understood as a differential ratio of the BP to FP rates in the dc limit,

$$\alpha_d = \frac{dP_{b0}}{dP_{f0}} = \frac{dI_{b0}}{dI_{f0}}, \quad (12)$$

because of the continuity of particle flow,

$$\Delta P_{f0} - \Delta P_{b0} = \frac{\Delta N_{C0}}{\tau_r}. \quad (13)$$

Energy relaxation times, τ_e , for injected electrons with excess energies are short, < 100 psec, enough to accomplish quickly the stationary Fermi-Dirac distribution of an electron temperature, T_e .²⁸ Hence, the parameters α_0 and α_d may be written as functions of the electron population N_{C0} , electron temperature T_e , and n -side barrier height $e\phi_n$ of the active region shown in Fig. 1. Such short energy relaxation times may justify the independence of the differential ratio α_d on the frequency over the entire range, $f \leq 100$ MHz, in the present work, allowing us the use of the same parameter α_d in Eqs. (10) and (11). Note, however, that the differential ratio α_d is, in general, not necessarily equal to the dc ratio α_0 .

The explicit expression for the spectral Fano factor of the photon number detected by a PD in the case of high-impedance noise suppression can be easily obtained by solving quantum-mechanical Langevin equations, as shown in Appendix A, and is given by

$$F_d(f) = 1 - \eta \frac{1 + \frac{2(1 - \alpha_d)}{1 - \alpha_0} (\alpha_d - \alpha_0) (2\pi f \tau_{te})^2}{1 + 2\alpha_d (2\pi f \tau_r) (2\pi f \tau_{te}) + (1 - \alpha_d)^2 (2\pi f \tau_r)^2 (2\pi f \tau_{te})^2 + (2\pi f \tau_r)^2 + (2\pi f \tau_{te})^2}, \quad (14)$$

where f is the frequency and the junction-response time τ_{te} is related to α_0 and α_d as $\tau_{te} = C_{dep} r_d = C_{dep} n k_B T (1 - \alpha_0) / \{e I_{LED} (1 - \alpha_d)\}$, within the framework of the thermionic FP and BP model, as will be derived in the next subsection, Sec. IV B [see Eq. (23)]. Equation (14) leads to the squeezing bandwidth (3-dB rolloff bandwidth) f_c ,

$$(2\pi f_c)^2 = \frac{1}{2(1 - \alpha_d)^2 \tau_r^2 \tau_{te}^2} \left[- \left\{ \tau_r^2 + \tau_{te}^2 + 2\alpha_d \tau_r \tau_{te} - \frac{4(1 - \alpha_d)}{1 - \alpha_0} (\alpha_d - \alpha_0) \tau_{te}^2 \right\} + \sqrt{\left\{ \tau_r^2 + \tau_{te}^2 + 2\alpha_d \tau_r \tau_{te} - \frac{4(1 - \alpha_d)}{1 - \alpha_0} (\alpha_d - \alpha_0) \tau_{te}^2 \right\}^2 + 4(1 - \alpha_d)^2 \tau_r^2 \tau_{te}^2} \right]. \quad (15)$$

In the case of $\alpha_0 = \alpha_d = 0$, Eq. (14) reduces to a form described by the product of two Lorentzians,

$$F_d(f) = 1 - \eta \frac{1}{\{1 + (2\pi f \tau_{te})^2\} \{1 + (2\pi f \tau_r)^2\}}, \quad (16)$$

and Eq. (15) reduces to

$$(2\pi f_c)^2 = \frac{1}{2\tau_r^2 \tau_{te}^2} \left\{ -(\tau_r^2 + \tau_{te}^2) + \sqrt{\tau_r^4 + \tau_{te}^4 + 6\tau_r^2 \tau_{te}^2} \right\}. \quad (17)$$

On the other hand, in another extreme case of $\alpha_0 = \alpha_d \rightarrow 1$, Eq. (14) reduces to a simpler form described by a single Lorentzian,

$$F_d(f) = 1 - \eta \frac{1}{1 + \{2\pi f (\tau_{te} + \tau_r)\}^2}, \quad (18)$$

and Eq. (15) leads to

$$f_c = \frac{1}{2\pi (\tau_{te} + \tau_r)}, \quad (19)$$

which is nothing but Eq. (1). In the former case, $\alpha_0 = \alpha_d = 0$, the FP and recombination processes in a diode can be viewed as being two cascade processes since no BP process exists at all. This case may be termed the thermionic-emission limit. On the contrary, in the latter case, $\alpha_0 = \alpha_d \rightarrow 1$, both the pump and recombination processes are completely linked so that they are inseparable from each other. This is the so-called macroscopic diffusion limit, discussed in Ref. 22.

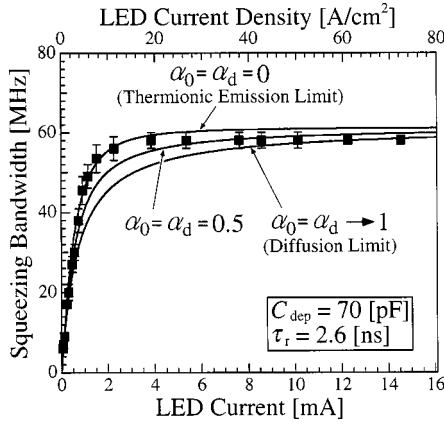


FIG. 7. Pump-current (-density) dependence of the observed squeezing bandwidth compared with the theoretical curves including the effects of backward-pump (BP) process. The theoretical curves for three different values of $\alpha_0 = \alpha_d = 0, 0.5,$ and 1 estimated with Eq. (15) by assuming $\tau_{te} = C_{dep} k_B T / (e I_{LED})$ are indicated. The values of junction capacitance and recombination lifetime used for the estimation are the same as in Fig. 6.

Let us presume that the BP rate P_b is a linear function of the electron population, N_C , i.e., $\alpha_d = \alpha_0 = \text{const}$. In Fig. 7, the experimental result of the squeezing bandwidth, f_c , is compared with three theoretical curves estimated with Eq. (15) by setting $\tau_{te} = C_{dep} k_B T / (e I_{LED})$ and by using the different constant values $0, 0.5,$ and 1 of α_0 and α_d and the same values of C_{dep} and τ_r as in Fig. 6. With the increasing pump current I_{LED} , the experimental f_c begins to deviate from the theoretical curve labeled $\alpha_0 = \alpha_d = 0$ [Eq. (17)] at $I_{LED} = 4$ mA, and eventually approaches the curve labeled $\alpha_0 = \alpha_d \rightarrow 1$ [Eq. (19)], suggesting that both α_0 and α_d are no longer constant but increasing functions of I_{LED} . In other words, the pump situation of our LED moves from the thermionic-emission toward diffusion limits as I_{LED} increases.

Here, we briefly discuss the possible current dependence of the parameters α_0 and α_d in a heterojunction diode, in comparison with a homojunction diode. In a homojunction diode, injected electrons may easily go back, causing $\alpha_0 = \alpha_d \rightarrow 1$, as discussed in Ref. 22. On the other hand, in a heterojunction diode as in the present diode, the BP process for injected electrons may be less significant than in the homojunction diode since the n -side potential barrier $e\phi_n$ formed by band-gap discontinuity of the heterojunction may block the backward transport of injected electrons. However, the BP rate may be superlinearly increased by band-filling and/or the hot carrier effect as I_{LED} increases, as already pointed out in the early part of this subsection. The superlinear increase in the BP rate yields increasing α_0 and α_d with I_{LED} , which will be, indeed, demonstrated in the next subsection.

B. Pump-current dependence of α_0 and α_d

In order to determine, independent of the noise measurements, the dependence of α_0 and α_d on the pump current I_{LED} , we measured the current-versus-voltage (I - V) characteristic and differential resistance of the LED used in the noise measurements. With the definition of α_0 , Eq. (7), if both the electron FP and BP events take place through ther-

mal emission over the p - n junction barrier as in heterojunction LEDs at room temperature, the net average current $I_{LED} (\equiv I_0)$ of a sufficiently strong forward-biased [$eV_{j0} / (nk_B T) \gg 1$] LED may be written as, taking account of the BP process,

$$I_{LED} = I_s \left\{ \exp\left(\frac{eV_{j0}}{nk_B T}\right) [1 - \alpha_0(V_{j0})] - 1 \right\} \\ \approx I_s \left\{ \exp\left(\frac{eV_{j0}}{nk_B T}\right) [1 - \alpha_0(V_{j0})] \right\}, \quad (20)$$

where I_s , V_{j0} , and n are the reverse saturation current, the average junction voltage across the n -type wide gap and p -type active regions, and the ideality factor, respectively. The factor n is slightly larger than unity, $1 \leq n \leq 1.2$, in the LEDs used in the present experiments. The deviation of n from unity may not only be due to recombination processes in the depletion layer, but due to carrier transport through graded-gap heterojunctions as clarified in Appendix B. Obviously, the parameter α_0 as a function of V_{j0} is identical to the one originally defined as functions of N_{C0} and T_e in the preceding subsection. This is because N_{C0} and T_e are uniquely determined by the dc junction voltage, V_{j0} , i.e., α_0 is an implicit function of V_{j0} . Equation (20) gives the differential junction resistance of the diode,

$$r_{dj} = \frac{nk_B T}{e I_{LED}} \frac{1 - \alpha_0(V_{j0})}{1 - \alpha_d(V_{j0})} = \frac{nk_B T}{e I_{LED}} \left(1 + \frac{nk_B T}{e} \frac{d\alpha_0(V_{j0})}{dV_{j0}} \frac{1}{1 - \alpha_d(V_{j0})} \right), \quad (21)$$

where $\alpha_d(V_{j0})$ is defined as

$$\alpha_d(V_{j0}) = \alpha_0(V_{j0}) + \frac{nk_B T}{e} \frac{d\alpha_0(V_{j0})}{dV_{j0}}. \quad (22)$$

The definition, Eq. (22), for α_d is easily confirmed to be identical to Eq. (12), $\alpha_d = dI_{b0} / dI_{f0} = (dI_{b0} / dV_{j0})(dV_{j0} / dI_{f0})$, because of $I_{f0} = I_s \exp\{eV_{j0} / (nk_B T)\}$ and $I_{b0} = I_s \alpha_0(V_{j0}) \exp\{eV_{j0} / (nk_B T)\}$. Equation (21) leads to the junction-response time,

$$\tau_{te} = C_{dep} r_{dj} = \frac{C_{dep} nk_B T}{e I_{LED}} \frac{1 - \alpha_0(V_{j0})}{1 - \alpha_d(V_{j0})}. \quad (23)$$

Note that in the LED used in the present work, $\alpha_d(V_{j0})$ is larger than $\alpha_0(V_{j0})$, since $\alpha_0(V_{j0})$ is an increasing function of V_{j0} , as will be demonstrated soon.

In an actual diode, we should take care about the influence of an internal series resistance r_s , involved in the diode (not R_s in the external circuit), on the I - V characteristic. If a voltage drop in the series resistance r_s is taken into account, Eq. (20) is rewritten as a function of $V_{meas} - I_{LED} r_s$,

$$I_{LED} = I_s \exp\left\{ \frac{e(V_{meas} - I_{LED} r_s)}{nk_B T} \right\} [1 - \alpha_0(V_{meas} - I_{LED} r_s)], \quad (24)$$

where V_{meas} is the measurable dc voltage applied between terminals of the device. Thus, both the r_s and α_0 pull down the values of I_{LED} from the simple exponential dependence.

The measurable differential resistance $r_{d,\text{meas}}$ is also affected by the presence of the internal series resistance, r_s , since we can measure only the sum of r_{dj} and r_s ,

$$r_{d,\text{meas}} = r_{dj} + r_s = \frac{nk_B T}{e I_{\text{LED}}} \left(1 + \frac{nk_B T}{e} \frac{d\alpha_0(V_{j0})}{dV_{j0}} \right) + r_s. \quad (25)$$

Since the second term, representing the influence of BP, in the parentheses on the right-hand side is positive, not only the voltage drop in the series resistance but also the BP process bring about an increase in $r_{d,\text{meas}}$. This point has not always been recognized so far. Rather, the deviation of I_{LED} from a simple exponential function of V_{meas} and that of $r_{d,\text{meas}}$ from the $1/I_{\text{LED}}$ dependence have been so far believed to be mainly due to the voltage drop in a series resistance of a diode.²⁹

Equations (24) and (25) indicate that it is not easy to separate the effects of the BP process and series resistance on I - V and r_d characteristics of the LED unless the value of r_s is known. Fortunately, however, the r_s value can be identified precisely in the following way. Equation (25) indicates that the influence of the BP process on $r_{d,\text{meas}}$ becomes less important at lower temperature. More importantly, the α_0 and α_d themselves decrease with decreasing temperature, as will be demonstrated later. Therefore, at a low temperature, $T \leq 70$ K, $r_{d,\text{meas}}$ in the high current regime would be governed by the internal series resistance r_s ($r_s \gg r_{dj}$). Figures 8(a) and 8(b) show the differential resistance of the diode, $r_{d,\text{meas}}$, measured at two ambient temperatures [room temperature (292 K) and low temperature (< 61 K)], as functions of I_{LED} . In the experiments, we carefully controlled the device temperature by mounting the LED on a heat sink. Indeed, with the luminescence spectra, the device (lattice) temperature was confirmed to be unchanged with increasing I_{LED} up to 20 mA. The differential resistance measured at low temperature, $T \leq 61$ K, can be fitted by the dotted straight line obtained with the differential junction resistance for $\alpha_0 = \alpha_d = 0$, $r_{dj,0} = nk_B T / (e I_{\text{LED}})$ by using $nT = 61$ K only in the very low current regime $I_{\text{LED}} < 0.1$ mA. In other words, the low temperature $r_{d,\text{meas}}$, obviously, deviates from the straight line in the higher current regime. Rather, the measured differential resistance is perfectly fitted over the entire current range with the dotted curve estimated by $r_{dj,0} + r_s$ with $nT = 61$ K and $r_s = 1.9 \Omega$. This convinces us that the internal series resistance r_s is identified to be 1.9Ω at the low temperature.

On the other hand, at room temperature, over the wider current range, $I_{\text{LED}} \leq 1.0$ mA, the measured differential resistance is closer to the solid straight line estimated with $r_{dj,0} = nk_B T / (e I_{\text{LED}})$ by using $T = 292$ K and $n = 1.08$, rather than the solid curve, $r_{dj,0} + 1.75 \Omega$, as shown in Fig. 8(a) and in more detail in Fig. 8(b) where the r_s value, 1.75Ω , was chosen tentatively to represent the experimental result at the highest I_{LED} . This indicates that the series resistance r_s at room temperature should be viewed as being much lower than the differential junction resistance $r_{dj,0} = nk_B T / (e I_{\text{LED}})$ in the wider current range. In fact, the room-temperature data up to $I_{\text{LED}} = 1$ mA are better represented by the dash-dotted curve estimated with $r_{dj,0} + r_s$ by

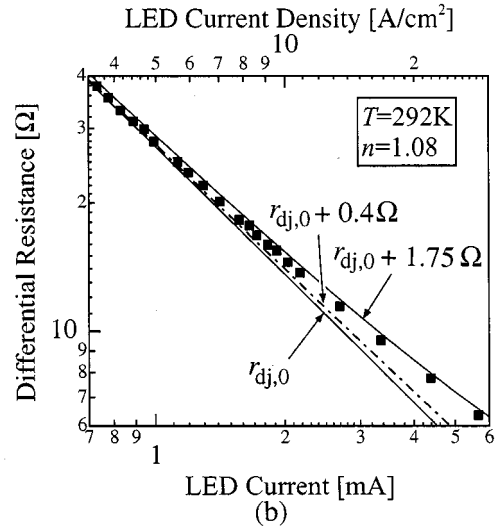
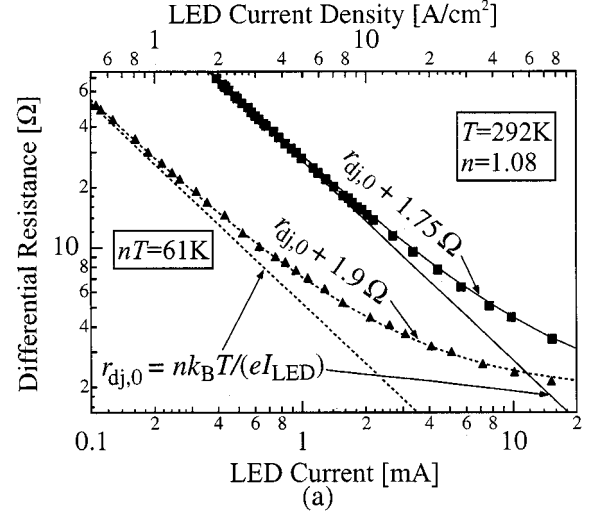


FIG. 8. (a) Measured differential resistance of the light-emitting diode (LED) as functions of pump current (density) at two different ambient temperatures [room temperature (292 K) and low temperature (< 61 K)]. (b) Enlarged plots of measured differential resistance at 292 K for a detailed comparison with theoretical values. The room-temperature data are compared with the solid straight line estimated with $r_{dj,0} = nk_B T / (e I_{\text{LED}})$ by using $T = 292$ K and $n = 1.08$ and the solid and dashed curves estimated with $r_{dj,0} + r_s$ by using $T = 292$ K, $n = 1.08$, and $r_s = 1.75 \Omega$, and $r_s = 0.4 \Omega$, respectively. The low-temperature data are compared with the dotted line estimated with $r_{dj,0} = nk_B T / (e I_{\text{LED}})$ by using $nT = 61$ K and the dotted curve estimated with $r_{dj,0} + r_s$ by using $nT = 61$ K and $r_s = 1.9 \Omega$.

using $T = 292$ K, $n = 1.08$, and $r_s = 0.4 \Omega$, indicating that the series resistance r_s at $T = 292$ K is much lower than that ($r_s = 1.9 \Omega$) at $nT = 61$ K. This is quite consistent with experimental results of the temperature dependence of resistivity in p - $\text{Al}_x\text{Ga}_{1-x}\text{As}$ as follows.

Figure 9(a) shows the schematic diagram of the cross-sectional structure of the LED.^{25,31} The thick i -type layer of $300 \mu\text{m}$ is shaped hemispherically to prevent the internal reflection of the ray emanating from the p -type active layer of $0.5\text{-}\mu\text{m}$ thickness. The junction radius of this device is $80 \mu\text{m}$. The p -type $\text{Al}_{0.2}\text{Ga}_{0.8}\text{As}$ layer of $30\text{-}\mu\text{m}$ thickness

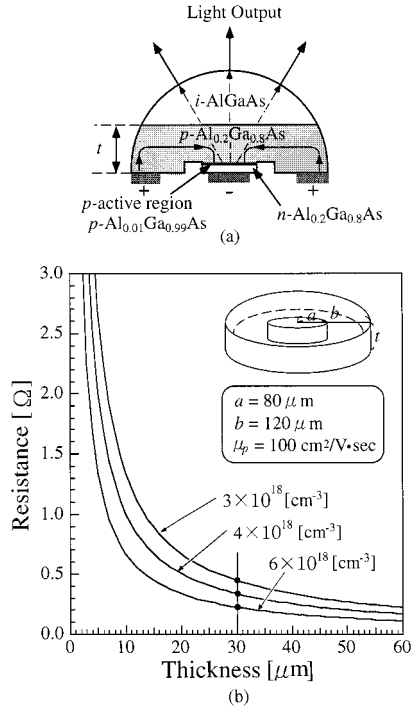


FIG. 9. (a) Schematic diagram of the cross-sectional structure of the p - n heterojunction light-emitting diode (LED). (b) Series resistance of the LED estimated based on a cylindrical-electrode model for three different hole concentrations (3 , 4 , and $6 \times 10^{18} \text{ cm}^{-3}$) as functions of thickness of the modeled p -type $\text{Al}_{0.2}\text{Ga}_{0.8}\text{As}$ layer.

was doped $(3-5) \times 10^{18} \text{ cm}^{-3}$, and the distance between the n - and p -side contact electrodes was designed to be about $80 \mu\text{m}$. Thus, the resistance for lateral current in the p -type $\text{Al}_{0.2}\text{Ga}_{0.8}\text{As}$ may dominate over the resultant series resistance r_s of the LED.²⁵ The temperature dependence of the hole concentration and mobility in p -type $\text{Al}_x\text{Ga}_{1-x}\text{As}$ with various Al-mole fractions x and doping levels has been extensively investigated in Ref. 30. According to their experimental results,³⁰ the resistance in the p -doped $[(3-5) \times 10^{18} \text{ cm}^{-3}] \text{ Al}_{0.2}\text{Ga}_{0.8}\text{As}$ layer at room temperature would be smaller by a factor of 10 than that at 61 K. In this view, the r_s at 292 K can be convincingly evaluated to be low, $\sim 0.2 \Omega$, since the series resistance at the low temperature is already identified to be 1.9Ω . As a cross check, we estimated the internal series resistance r_s based on a cylindrical-electrode model for the p -type wide-band-gap layer in the present LED illustrated in the inset of Fig. 9(b). The resistance between the inner and outer walls of the cylinder is expressed as

$$r_s = \int_a^b \rho \frac{dr}{2\pi r t} = \frac{\rho}{2\pi t} \ln \frac{b}{a}, \quad (26)$$

where a , b , t , and ρ are the inside radius, the outside radius, the thickness, and the resistivity of the material, respectively. For the geometrical parameters of our LED,^{25,31} $a = 80 \mu\text{m}$ and $b = 120 \mu\text{m}$, and the typical hole mobility³⁰ at room temperature, $\mu_p = 100 \text{ cm}^2/\text{V sec}$, we plotted in Fig. 9(b) the estimated resistance as functions of thickness, t , of the p -type layer of three different (possible) hole concentrations

(3 , 4 , and $6 \times 10^{18} \text{ cm}^{-3}$). The resistance $0.2-0.5 \Omega$ estimated with a standard thickness $30 \mu\text{m}$ of the p -type layer,²⁵ is reasonably close to the value evaluated earlier, $\sim 0.4 \Omega$.

Now, let us step back to Figs. 8(a) and 8(b). Presumably, suppose that the observed differential resistance $\sim 3.0 \Omega$ in the highest current, $I_{\text{LED}} = 20 \text{ mA}$, at room temperature is mainly attributable to a fixed series resistance, as concluded in Ref. 25. At first sight, the assumption leads to a fitting, particularly in the high current regime, $I_{\text{LED}} \geq 8 \text{ mA}$, between the experiment data and the theoretical solid curve obtained with $r_{dj,0} + r_s$ of $T = 292 \text{ K}$, $n = 1.08$, and $r_s = 1.75 \Omega$, as shown in the figures. However, in addition to the discrepancy shown in Fig. 8(b), the series-resistance ($r_s = 1.75 \Omega$) model without the BP process brings us a failure in the interpretation of the observed current dependence of squeezing cutoff frequency since such a postulated internal series resistance much lower than the external series resistance, $R_s = 2 \text{ K}\Omega$, in the external circuit may not affect appreciably the noise characteristics of photon fluxes. In this view, the conclusion on the internal series resistance made in Ref. 25 is misleading.³² As a consequence, one has to look for a different circuit model, namely a parallel circuit model in which an unknown resistance r_x is, in parallel, connected to the resistance, $r_{dj,0} = nk_B T / (eI_{\text{LED}})$. In such a case, the unknown resistance r_x should be *negative*. Otherwise, $r_{d,\text{meas}}$ is lower than $nk_B T / (eI_{\text{LED}})$ unlike the experimental results because the resultant conductance in the parallel circuit, $1/r_{dj,0} + 1/r_x$, is higher than $1/r_{dj,0}$ for a positive r_x . Thus, it turns out that the *negative* differential resistance r_x suggests definitely the existence of the BP process.

Once the r_s values are identified, one can easily obtain the current-versus-junction-voltage (I - V_{j0}) characteristics from the measured current-versus-voltage (I - V_{meas}) characteristics shown in Fig. 10(a) by using the relation $V_{j0} = V_{\text{meas}} - r_s I_{\text{LED}}$ with $r_s = 0.4 \Omega$ at $T = 292 \text{ K}$ and $r_s = 1.9 \Omega$ at $nT = 61 \text{ K}$. Figure 10(b) shows the I - V_{j0} characteristics at two temperatures. The straight lines represent the theoretical prediction, $I_{\text{LED}} = I_s \exp\{eV_{j0}/(nk_B T)\}$, without BP currents, i.e., $\alpha_0(V_{j0}) = 0$. Obviously, the experimental results for $T < 61 \text{ K}$ are fitted excellently by the dashed straight line, obtained with $nT = 61 \text{ K}$, over two-orders-of-magnitude change in I_{LED} , indicating that no BP process exists at all at such a low temperature. On the other hand, the results for 292 K still show deviation from the solid straight line, obtained with $T = 292 \text{ K}$ and $n = 1.08$. The discrepancy at 292 K, in turn, clearly manifests the existence of the BP process.

The dependence of α_0 on V_{j0} at room temperature can be deduced with the results of the I - V_{j0} characteristic and differential resistance by using Eqs. (20)–(22), as follows. Referring to Fig. 10(b), by assuming $\alpha_0 = 0$ in the low current regime $I_{\text{LED}} \leq 1 \text{ mA}$, consistent with the results of noise measurements shown in Fig. 7, the ratio of the experimental value of I_{LED} to the theoretical one, $I_{\text{LED}} \propto \exp\{eV_{j0}/(nk_B T)\}$, gives us $\alpha_0(V_{j0})$, i.e., for instance, $I_1/I_2 = 1 - \alpha_0(V_{j0})$. The V_{j0} dependence of α_d can be determined from the obtained V_{j0} dependence of $\alpha_0(V_{j0})$ through the use of Eq. (22) or by use of the values of α_0 and $r_{dj}(=r_{d,\text{meas}} - r_s)$ in Eq. (21). Figure 11 shows the obtained I_{LED} dependence of α_0 and α_d at room temperature. The BP process begins to show up at

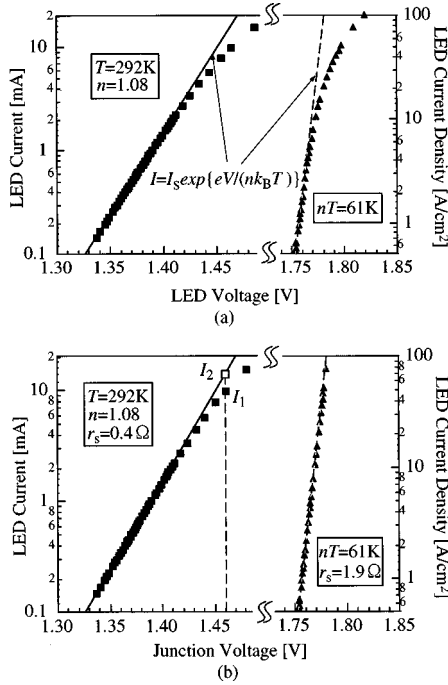


FIG. 10. (a) Measured current-vs-voltage (I - V_{meas}) characteristics of the light-emitting diode (LED) at the same temperatures as in Fig. 8, which are compared with $I_{\text{LED}} = I_s \exp\{eV_{j0}/(nk_B T)\}$ (straight lines) without BP currents. The device temperatures and ideality factors are used to be the same as in Fig. 8. (b) Current-vs-junction-voltage (I - V_{j0}) characteristics of the LED obtained from I - V_{meas} characteristics by using $V_{j0} = V_{\text{meas}} - r_s I_{\text{LED}}$. These are also compared with the same straight lines as in (a).

about $I_{\text{LED}} \approx 1$ mA and α_d is always larger than α_0 , as has already been anticipated. Physics underlying the obtained current dependence of the BP parameters, α_0 and α_d , will be discussed elsewhere³³ based upon microscopic models such as the hot electron effect and state filling in tailed states of a conduction band in the active alloy material, $\text{Al}_{0.01}\text{Ga}_{0.99}\text{As}$.

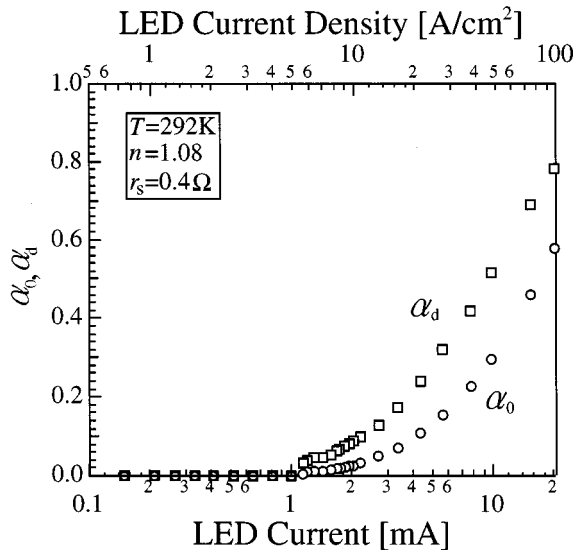


FIG. 11. Pump-current (-density) dependence of the dc and differential ratios of backward- (BP) to forward-pump (FP) rates, α_0 and α_d , determined independently of noise measurements.

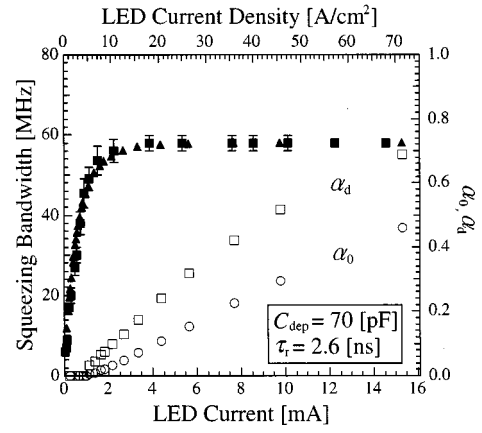


FIG. 12. Pump-current (-density) dependence of squeezing bandwidth (squares) compared with theoretical values (triangles) estimated with Eq. (15) together with Eq. (23) by using the pump-current dependence of α_0 and α_d shown in Fig. 11. In the estimation, the junction capacitance and recombination lifetime are used to be the same as in Figs. 6 and 7. The values for α_0 and α_d are also shown.

C. Bandwidth for the noise suppression

The experimental results of the squeezing bandwidth can be compared with our theory, Eq. (15), by using the pump-current dependence of α_0 and α_d , obtained in the preceding subsection. Figure 12 shows the experimental result (closed squares) of the pump-current dependence of the squeezing bandwidth at room temperature in comparison with theoretical values (closed triangles) estimated by Eq. (15) together with Eq. (23) by using the same values of C_{dep} and τ_r as in Figs. 6 and 7 as well as $n = 1.08$ and $T = 292$ K and the obtained α_0 and α_d again plotted in the figure. The experimental results are perfectly fitted over the whole range of pump current by the theoretical ones taking account of the increasing α_0 and α_d with increasing pump current. The agreement between the experimental and theoretical results estimated with α_0 and α_d deduced from dc measurements of I - V characteristic and differential resistance indicates that the independence of α_d on frequency, assumed in Sec. IV A, is justified. Furthermore, it should be stressed that our noise measurements have been done under a quite standard condition, namely a commercial LED operating at low current density (0.3–72 A/cm²) and at room temperature. In other words, the movement of the pump condition from thermionic emission ($\alpha_0 = \alpha_d = 0$) toward the diffusion limit ($\alpha_0 = \alpha_d \rightarrow 1$) with increasing pump current would be commonly seen in heterojunction LEDs.

In order to visualize more clearly the existence of the BP process and the difference in the squeezing bandwidth between the thermionic emission and diffusion limits, the following experiment at room temperature has been carried out. The difference becomes most sizable when the time constants of pump and recombination dynamics are comparable, namely at $I_{\text{LED}} = 1$ –3 mA in the case of Fig. 7 or Fig. 12. The parallel capacitances C_p have been connected to the LED driven at two different pump currents, $I_{\text{LED}} = 3.2$ mA ($\alpha_0 = 0.06$ and $\alpha_d = 0.16$) and 12.0 mA ($\alpha_0 = 0.37$ and $\alpha_d = 0.60$), to artificially change the junction-response time of the LED, defined as $\tau_{\text{eff},0} = nk_B T (C_{\text{dep}}$

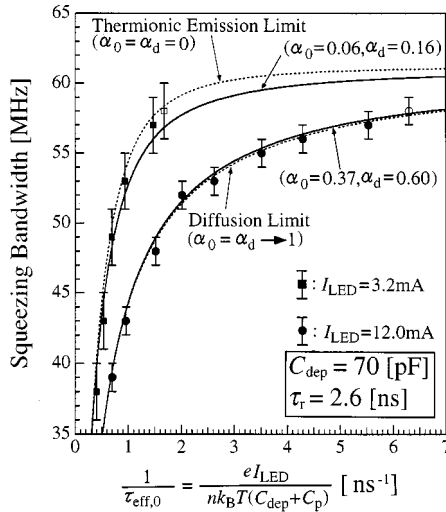


FIG. 13. Experimental squeezing bandwidth, controlled by the parallel connection of external capacitances, C_p , to the light-emitting diode (LED) driven at two different pump currents ($I_{\text{LED}} = 3.2$ mA and 12.0 mA) plotted as functions of the inverse of junction-response time, $1/\tau_{\text{eff},0} = eI_{\text{LED}} / \{nk_B T(C_{\text{dep}} + C_p)\}$. $\tau_{\text{eff},0}$ is obtained by using $T = 292$ K, $n = 1.08$, and $C_{\text{dep}} = 70$ pF. The open circle and square represent the squeezing bandwidths at each pump current in the case of $C_p = 0$. The experimental results are compared with four theoretical curves. On the estimation procedures of the theoretical curves, see the text.

$+ C_p) / (eI_{\text{LED}})$. Thus, the dependence of the squeezing bandwidth at the fixed bias points (the fixed BP rates, i.e., the fixed α parameters) on $\tau_{\text{eff},0}$ can be investigated. Figure 13 shows the experimental squeezing bandwidth plotted as functions of $1/\tau_{\text{eff},0}$ estimated by using $T = 292$ K, $n = 1.08$, and $C_{\text{dep}} = 70$ pF, and the open circle and square in the figure represent the squeezing bandwidths in the case of $C_p = 0$. The experimental results are compared with four theoretical curves as functions of $1/\tau_{\text{eff},0}$ which are estimated by Eq. (17) (thermionic-emission limit, $\alpha_0 = \alpha_d = 0$), Eq. (19) (diffusion limit, $\alpha_0 = \alpha_d \rightarrow 1$), and Eq. (15) with α_0 and α_d values at each bias point, all with $\tau_r = 2.6$ ns. Also, in the equations the junction-response time τ_{te} originally given by Eq. (23) is replaced by the effective value, $\tau_{\text{te,para}} = nk_B T(C_{\text{dep}} + C_p)(1 - \alpha_0) / \{eI_{\text{LED}}(1 - \alpha_d)\}$. The experimental squeezing bandwidth decreases with the increasing parallel capacitance, namely increasing $\tau_{\text{eff},0}$. The squeezing bandwidth at each pump current is well fitted by the corresponding theoretical solid curves estimated with α_0 and α_d at each bias point. Especially, as far as the squeezing bandwidth is concerned, the LED driven at $I_{\text{LED}} = 3.2$ mA behaves as if in the thermionic-emission limit whereas the LED driven at $I_{\text{LED}} = 12.0$ mA behaves as if in the diffusion limit. Furthermore, the agreement between the theoretical and experimental results indicates that the internal series resistance of the LED is very low at room temperature, $r_s \ll r_{dj}$. Otherwise, the experimental results plotted against $1/\tau_{\text{eff},0}$, which is defined under the assumption that the capacitance C_p is connected in parallel directly to the p - n heterojunction, would never be fitted by the theoretical curves. Thus, the internal series resistance r_s at room temperature is convinc-

ingly concluded to be much lower than the differential junction resistance, $r_{dj} = 3.6 \Omega$, even at the high current $I_{\text{LED}} = 12.0$ mA.

V. CONCLUSIONS

In this work, we have investigated experimentally and theoretically the bandwidth for the squeezing of photon-number fluctuations in constant-current-driven heterojunction LEDs operating at room temperature, focusing on the driving-current dependence of the bandwidth. The experiments using high-performance (high-speed, highly efficient) $\text{Al}_x\text{Ga}_{1-x}\text{As}$ LEDs carried out with careful measurements have led to the observation of apparent squeezing up to 100 MHz and allowed us a precise quantitative comparison with the theory.

In low and high injection current regimes, the squeezing bandwidths have been explained well to be limited by the response time of the p - n junction and the recombination lifetime in the active region, respectively, as already pointed out in previous work. However, it has been found in the present work that, in the intermediate current region, previous theory including the FP and BP processes in the diffusion limit, originally developed for homojunction LEDs, fails to interpret the experimental results. We have proposed a theoretical model, generally applicable to heterojunction LEDs, where the dc and ac ratios of the BP to FP rates are included as parameters α_0 and α_d . It has been revealed that changes in the pump situation are included in a quite natural manner in the expression for the squeezing bandwidth, and as a consequence that the transition of the situation from thermionic emission to diffusion limits associated with the changes of α_0 and α_d appears as the change of the bandwidth. The α_0 and α_d values have been determined by the measurements of current-versus-voltage characteristic and the differential resistance of the LED, and demonstrated to increase with the pump current. By the uses of these obtained α_0 and α_d values, the experimental results of injection-current dependence of the squeezing bandwidth have been represented quite excellently, over the whole range of the injection current used in the noise measurements. In particular, the experimental results of the squeezing bandwidth obtained with slowing down of the junction-response speed by the parallel connection of external capacitances have very clearly supported the present model. Hence, we conclude that the BP process plays an essentially important role in the photon-number squeezing in heterojunction LEDs and the pump-current dependence of the squeezing bandwidth manifests the transition of carrier transport across the p - n heterojunction, from thermionic emission to diffusion limits. The present experiments carried out with commercially available LEDs under a very standard operating condition have indicated the general importance of the BP process in heterojunction LEDs and demonstrated that careful noise measurements reveal the transition of the pump situation prominently, and, in turn, give insights into general device characteristics of LEDs such as dynamic response for external current modulation.

In this paper, the discussion has been mainly focused on the microscopic carrier injection process. However, the electron recombination process as well as the pump process may certainly affect the photon-number squeezing in semiconduc-

tor light emitters. The squeezing bandwidth in the relatively high pump-current regime is limited by the radiative recombination dynamics in the active region. Namely, the shortening of the radiative lifetime may lead to the wider-band squeezing in a LED. In fact, by adopting the modulation-doping scheme to the active region as a technical way to shorten the radiative lifetime, we very recently have demonstrated the photon-number squeezing over 300 MHz in a LED driven at room temperature,³⁴ rather close to the bandwidth observed with LDs.^{2,4}

ACKNOWLEDGMENTS

The authors would like to thank H. Taniguchi for the installation of the shield room used in the present work. We are also grateful to T. Hirano and J. Abe for their helpful discussions. A part of this work has been supported by Scientific Research Grant-in-Aids (Grant No. 10555018) from the Ministry of Education, Science and Culture of Japan.

APPENDIX A: EXPRESSION FOR THE PHOTON NOISE POWER SPECTRAL DENSITY OF AN LED DRIVEN BY A CONSTANT-CURRENT SOURCE

In this appendix, we derive the expression for noise power spectral density of the photon-number fluctuations on the basis of quantum-mechanical Langevin equations including the effects of the BP process.

A junction voltage change in the LED induced by the FP and BP events is represented, using Eqs. (3) and (4), by

$$\begin{aligned} & - \int \frac{e[\hat{P}_f(t) + \hat{\Gamma}_{\text{pf}}(t) - \hat{P}_b(t) - \hat{\Gamma}_{\text{pb}}(t)]}{C_{\text{dep}}} dt \\ & = - \int \frac{e(P_{f0} - P_{b0})}{C_{\text{dep}}} dt \\ & - \int \frac{e[\Delta\hat{P}_f(t) - \Delta\hat{P}_b(t) + \hat{\Gamma}_{\text{pf}}(t) - \hat{\Gamma}_{\text{pb}}(t)]}{C_{\text{dep}}} dt, \end{aligned} \quad (\text{A1})$$

and the voltage change is recovered by continuous charging due to the external constant current $\hat{I}(t) = I_0$, with a constant rate,

$$\frac{I(t)}{C_{\text{dep}}} = \frac{I_0}{C_{\text{dep}}}. \quad (\text{A2})$$

Hence, the net voltage fluctuation is expressed as

$$\Delta\hat{V}_j = - \int \frac{e[\Delta\hat{P}_f(t) - \Delta\hat{P}_b(t) + \hat{\Gamma}_{\text{pf}}(t) - \hat{\Gamma}_{\text{pb}}(t)]}{C_{\text{dep}}} dt, \quad (\text{A3})$$

where we used

$$\frac{e(P_{f0} - P_{b0})}{C_{\text{dep}}} = \frac{I_0}{C_{\text{dep}}}. \quad (\text{A4})$$

This voltage fluctuation causes the small-amplitude fluctuation $\Delta\hat{P}_f(t)$ in the FP rate,

$$\Delta\hat{P}_f(t) = P_{f0} \exp\left(\frac{e\Delta\hat{V}_j}{nk_B T}\right) - P_{f0} \quad (\text{A5})$$

in the case of thermionic FP process, where n is the ideality factor. Linearization of Eq. (A5) leads to the quantum-mechanical Langevin equation for the FP rate fluctuation,

$$\Delta\hat{P}_f(t) \simeq - \frac{1}{\tau_{\text{tef}}} \int [\Delta\hat{P}_f(t) - \Delta\hat{P}_b(t) + \hat{\Gamma}_{\text{pf}}(t) - \hat{\Gamma}_{\text{pb}}(t)] dt, \quad (\text{A6})$$

or

$$\frac{d\Delta\hat{P}_f(t)}{dt} \simeq - \frac{1}{\tau_{\text{tef}}} [\Delta\hat{P}_f(t) - \Delta\hat{P}_b(t) + \hat{\Gamma}_{\text{pf}}(t) - \hat{\Gamma}_{\text{pb}}(t)], \quad (\text{A7})$$

where the thermionic-emission time for the FP process, τ_{tef} , is defined as

$$\tau_{\text{tef}} = \frac{nk_B T}{eI_{f0}} C_{\text{dep}} = (1 - \alpha_0) \frac{nk_B T}{eI_0} = (1 - \alpha_d) \tau_{\text{te}}. \quad (\text{A8})$$

In the derivation of the last relation in Eq. (A8), Eq. (23) in Sec. IV B was used. Fourier transformation of Eq. (A6) [or Eq. (A7)] leads to

$$\Delta\tilde{P}_f + \tilde{\Gamma}_{\text{pf}} = \frac{\Delta\tilde{P}_b + i\Omega\tau_{\text{tef}}\tilde{\Gamma}_{\text{pf}} + \tilde{\Gamma}_{\text{pb}}}{1 + i\Omega\tau_{\text{tef}}}, \quad (\text{A9})$$

where $\Omega = 2\pi f$ is the angular frequency. The Fourier component of the small-amplitude fluctuation $\Delta\hat{P}_b(t)$ of the BP rate operator, given by Eq. (10), leads to

$$\Delta\tilde{P}_b + \tilde{\Gamma}_{\text{pb}} = \frac{\alpha_d}{1 - \alpha_d} \frac{\Delta\tilde{N}_C}{\tau_r} + \tilde{\Gamma}_{\text{pb}}. \quad (\text{A10})$$

On the other hand, the quantum-mechanical Langevin equation for electron population operator $\hat{N}_C(t)$ in the active region is given by

$$\begin{aligned} \frac{d\hat{N}_C(t)}{dt} & = P_{f0} - P_{b0} + \Delta\hat{P}_f(t) - \Delta\hat{P}_b(t) + \hat{\Gamma}_{\text{pf}}(t) - \hat{\Gamma}_{\text{pb}}(t) \\ & - \frac{\hat{N}_C(t)}{\tau_r} - \hat{\Gamma}_{\text{sp}}(t), \end{aligned} \quad (\text{A11})$$

where $\hat{\Gamma}_{\text{sp}}(t)$ is the noise source operator associated with the spontaneous-emission process. Using Eq. (5) and $P_{f0} - P_{b0} = N_{C0}/\tau_r$ in Eq. (A11), one obtains

$$\begin{aligned} \frac{d\Delta\hat{N}_C(t)}{dt} & = \Delta\hat{P}_f(t) - \Delta\hat{P}_b(t) + \hat{\Gamma}_{\text{pf}}(t) - \hat{\Gamma}_{\text{pb}}(t) - \frac{\Delta\hat{N}_C(t)}{\tau_r} \\ & - \hat{\Gamma}_{\text{sp}}(t). \end{aligned} \quad (\text{A12})$$

Fourier transformation of Eq. (A12) together with the uses of Eqs. (A9) and (A10) leads to

$$\Delta\tilde{N}_C = \frac{\left\{ \frac{i\Omega\tau_{\text{tef}}}{1+i\Omega\tau_{\text{tef}}} (\tilde{\Gamma}_{\text{pf}} - \tilde{\Gamma}_{\text{pb}}) - \tilde{\Gamma}_{\text{sp}} \right\} \tau_r}{1+i\Omega\tau_r + \frac{\alpha_d}{1-\alpha_d} \frac{i\Omega\tau_{\text{tef}}}{1+i\Omega\tau_{\text{tef}}}}. \quad (\text{A13})$$

The quantum-mechanical Langevin equation for the photon flux operator $\hat{\Phi}(t)$ detected by a PD is given by

$$\hat{\Phi}(t) = \eta \frac{\hat{N}_C(t)}{\tau_r} + \hat{F}(t) = \eta \frac{N_{C0}}{\tau_r} + \eta \frac{\Delta\hat{N}_C(t)}{\tau_r} + \hat{F}(t), \quad (\text{A14})$$

where $\hat{F}(t)$ is the noise source operator associated with photon emissions detected by the PD. Here, we assume that the photon damping rate γ is infinite, which is justified in the usual LED cases. Thus, the noise power spectrum of output (detected) photon fluxes can be expressed as

$$\begin{aligned} 2\langle\Delta\tilde{\Phi}^\dagger\Delta\tilde{\Phi}\rangle &= 2\left\langle\left(\eta\frac{\Delta\tilde{N}_C^\dagger}{\tau_r} + \tilde{F}^\dagger\right)\left(\eta\frac{\Delta\tilde{N}_C}{\tau_r} + \tilde{F}\right)\right\rangle \\ &= \frac{2\eta^2}{\tau_r^2}\langle\Delta\tilde{N}_C^\dagger\Delta\tilde{N}_C\rangle + \frac{2\eta}{\tau_r}\langle\Delta\tilde{N}_C^\dagger\tilde{F}\rangle \\ &\quad + \frac{2\eta}{\tau_r}\langle\tilde{F}^\dagger\Delta\tilde{N}_C\rangle + 2\langle\tilde{F}^\dagger\tilde{F}\rangle, \end{aligned} \quad (\text{A15})$$

where the angular brackets $\langle \rangle$ stand for the bath averages of quantum-mechanical expectation values. The Markoffian correlation functions of various noise sources are obtained, by starting with the generalized Einstein (drift-diffusion) relations,³⁵ as

$$\langle\tilde{\Gamma}_{\text{pf}}^\dagger\tilde{\Gamma}_{\text{pf}}\rangle = \frac{1}{1-\alpha_0}P_0, \quad (\text{A16})$$

$$\langle\tilde{\Gamma}_{\text{pb}}^\dagger\tilde{\Gamma}_{\text{pb}}\rangle = \frac{\alpha_0}{1-\alpha_0}P_0, \quad (\text{A17})$$

$$\langle\tilde{\Gamma}_{\text{sp}}^\dagger\tilde{\Gamma}_{\text{sp}}\rangle = \frac{N_{C0}}{\tau_r}, \quad (\text{A18})$$

$$\langle\tilde{F}^\dagger\tilde{F}\rangle = \eta\frac{N_{C0}}{\tau_r}, \quad (\text{A19})$$

$$\langle\tilde{\Gamma}_{\text{sp}}^\dagger\tilde{F}\rangle = \langle\tilde{F}^\dagger\tilde{\Gamma}_{\text{sp}}\rangle = \eta\frac{N_{C0}}{\tau_r}. \quad (\text{A20})$$

The bath averages of all other cross-correlation functions are zero. Hence, one can obtain the spectral Fano factor for the constant-current-driven LED including the effect of the BP process by using Eqs. (A13) and (A15)–(A20),

$$F_d(f) = \frac{2\langle\Delta\tilde{\Phi}^\dagger\Delta\tilde{\Phi}\rangle}{2\eta P_0} = 1 - \eta \frac{1 + \frac{2(1-\alpha_d)}{1-\alpha_0}(\alpha_d - \alpha_0)(2\pi f\tau_{\text{te}})^2}{1 + 2\alpha_d(2\pi f\tau_r)(2\pi f\tau_{\text{te}}) + (1-\alpha_d)^2(2\pi f\tau_r)^2(2\pi f\tau_{\text{te}})^2 + (2\pi f\tau_r)^2 + (2\pi f\tau_{\text{te}})^2}, \quad (\text{A21})$$

where f is the frequency. This is Eq. (14) in Sec. IV A.

APPENDIX B: THE IDEALITY FACTOR IN THE CURRENT-VOLTAGE CHARACTERISTIC OF A GRADED-GAP HETEROJUNCTION LED

We discuss the ideality factor n , appearing in Eq. (20), in the graded-gap $\text{Al}_x\text{Ga}_{1-x}\text{As}$ heterojunction LED used in the present work in this appendix. Figure 14 shows the energy-band diagram of a p - n heterojunction with a band-gap grading, where the boundary between the p -type active region and n -type wide-band-gap regions is positioned at $z=0$. The graded-gap region may be formed due to so-called melt-back process in a temperature-gradient liquid phase epitaxy (LPE) by which the present LED was prepared.²⁵ When the doping concentration of the p -type layers is much higher than that of the n -type layer, $N_a \gg N_d$ as in the present LED, the average forward-current density J_{f0} of a strongly forward-biased LED within the framework of the thermionic FP model is given by

$$J_{f0} = J_A \exp\left\{\frac{-e[V_{Bn} - V_{j0} - \Delta(V_{j0})]}{k_B T}\right\}, \quad (\text{B1})$$

where J_A is the constant, V_{Bn} the built-in voltage in the case of an abrupt-gap junction as shown by the dashed line, and $\Delta(V_{j0})$ the lowering of peak energy of the potential barrier induced by the band-gap grading in the p - n junction. Linearization of the variation of $\Delta(V_{j0})$ with respect to the junction voltage change $V_{j0} - V_{j0}^{(0)}$ leads to $\Delta(V_{j0}) = \Delta_0 - \delta(V_{j0} - V_{j0}^{(0)})$, and then the effective built-in voltage in the graded-gap junction is given by $V_{Bn} - \Delta_0$, where Δ_0 is the peak-potential difference between the abrupt- and graded-gap heterojunctions at the specific bias voltage $V_{j0}^{(0)}$. As a result, Eq. (B1) can be written as

$$J_{f0} = J_s \exp\left\{\frac{eV_{j0}(1-\delta)}{k_B T}\right\}, \quad (\text{B2})$$

where $J_s = J_A \exp\{-e(V_{Bn} - \Delta_0 - \delta V_{j0}^{(0)})/(k_B T)\}$. Thus, the ideality factor n in Eq. (20) is given by $1/(1-\delta)$.

From the Poisson's equation, the potential $e\psi(z)$ for an electron in the graded-gap heterojunction can be represented to be, for $0 \leq z \leq d_{\text{dep}}$,

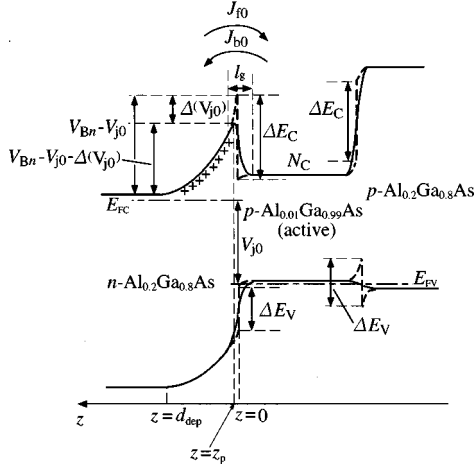


FIG. 14. Energy band diagram of an $\text{Al}_x\text{Ga}_{1-x}\text{As}$ p - n heterojunction with band-gap gradings (shown by solid lines) or without band-gap gradings (by dashed lines).

$$e\psi(z) = \frac{e^2 N_d}{\epsilon_0 \epsilon_r} \left(\frac{1}{2} z^2 - z d_{\text{dep}} \right) + \frac{\Delta E_C}{2} \left\{ 1 + \tanh \left(\frac{z}{l_g} \right) \right\}, \quad (\text{B3})$$

where ϵ_0 is the vacuum permittivity, ϵ_r the relative permittivity, $d_{\text{dep}} = \sqrt{2\epsilon_0\epsilon_r(V_{Bn} - V_{j0})/(eN_d)}$ the depletion layer width for the one-sided step junction ($N_a \gg N_d$), $\Delta E_C \{1 + \tanh(z/l_g)\}/2$ the position-dependent conduction-band offset between the n -type and active regions,³⁶ and l_g the grading width of the heterojunction. The conduction-band offset ΔE_C in the $\text{Al}_x\text{Ga}_{1-x}\text{As}$ system at room temperature is determined by the well-known Al-mole fraction x dependence of the band gap, $E_g = 1.424 + 1.247x$ eV,³⁷ and 70:30 rule for the ratio of conduction to valence-band offsets.³⁸ The electric charge, eN_d , due to ionized donors may be canceled partially by electron charges around the edge of the depletion layer $z \sim d_{\text{dep}}$, thus Eqs. (B1)–(B3) can be used only under the condition that the barrier height of the forward-biased graded-gap heterojunction is much higher than the thermal energy, i.e., $V_{Bn} - V_{j0} - \Delta(V_{j0}) \gg k_B T/e$. This condition is equivalent to one that the depletion layer width d_{dep} is much wider than the Debye length, $L_D = \sqrt{k_B T \epsilon_0 \epsilon_r / (e^2 n_e)}$, within which the Coulomb potential of ionized donors is screened by free electrons in the n -type region, where $n_e (\sim N_d)$ is the electron density in the n -type region.

The potential $e\psi(z)$ is maximized at the position, z_p , given by

$$\left(\frac{e^2 N_d}{\epsilon_0 \epsilon_r} \right) z_p + \left(\frac{\Delta E_C}{2l_g} \right) \text{sech}^2(z_p/l_g) = \left(\frac{e^2 N_d}{\epsilon_0 \epsilon_r} \right) d_{\text{dep}}, \quad (\text{B4})$$

allowing us the computation of junction-voltage dependence of the potential lowering Δ . Figure 15 shows the computed junction-voltage dependence of Δ at room temperature for the graded-gap $n(\text{Al}_{0.2}\text{Ga}_{0.8}\text{As})$ - $p(\text{Al}_{0.01}\text{Ga}_{0.99}\text{As})$ hetero-

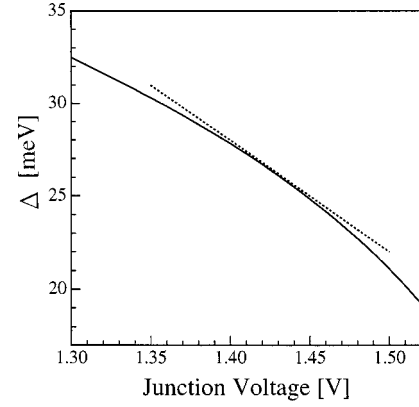


FIG. 15. Junction-voltage dependence of the computed lowering of barrier height, Δ , for the graded-gap $n(\text{Al}_{0.2}\text{Ga}_{0.8}\text{As})$ - $p(\text{Al}_{0.01}\text{Ga}_{0.99}\text{As})$ heterojunction with the grading width $l_g = 18$ Å and the donor doping density $N_d = 1 \times 10^{17}$ cm^{-3} , which is much lower than the acceptor doping density $N_a \sim 10^{18}$ cm^{-3} in the active region.

junction with the grading width $l_g = 18$ Å (Ref. 39) and the donor doping density $N_d = 1 \times 10^{17}$ cm^{-3} obtained with C - V measurements, which is much lower than the acceptor doping density, $N_a \sim 10^{18}$ cm^{-3} in the active region.²⁵ The peak potential difference Δ changes almost linearly with the junction voltage ($V_{j0} = 1.35$ – 1.5 V) used in the noise measurements. As a result, the ideality factor $n = 1.06$ obtained from the slope of dashed line for $V_{j0}^{(0)} = 1.43$ V shown in Fig. 15 is very close to that, $n = 1.08$, determined by I - V characteristic or differential resistance measurements at room temperature. It should be noted that the deviation of computed $\Delta(V_{j0})$ from the dotted straight line in Fig. 15 is too small (for instance, 0.5 meV at $V_{j0} = 1.48$ V $\ll k_B T \sim 25$ meV) to count the deviation from the straight line in the current-versus-junction-voltage characteristic at $T = 292$ K shown in Fig. 10(b).

The barrier height for electrons [$V_{Bn} - V_{j0} - \Delta(V_{j0})$] in the p - n junction under the driving conditions ($V_{j0} = 1.35$ – 1.5 V) of the LED in noise measurements is estimated to be 220–79 meV, which is much higher than $k_B T/e \approx 25$ meV. The n -side barrier height [$e\phi_n \approx \Delta E_C - \Delta(V_{j0})$] in the active region is obtained to be 136–145 meV so that electrons in the active region with energies higher than the n -side barrier height due to the hot carrier effect and/or band filling can go back to the n -type wide-band-gap region and, thus, BP current J_{b0} can flow. However, since the p -side barrier height ($\sim \Delta E_C + \Delta E_V \approx 237$ meV, where ΔE_V is the valence-band offset in the p - p junction) for injected electrons is unaffected by the existence of grading in the p - p junction, the p -side barrier height is always higher than the n -side one, $\Delta E_C + \Delta E_V > e\phi_n$. Thus, thermal emission of electrons to the p -type wide-band-gap region may not take place. This is a primary reason why the quantum efficiency of the present LED is maintained to be high despite the existence of a significant BP process.

- *Electronic address: yaman@ipc.hiroshima-u.ac.jp
- ¹Y. Yamamoto, S. Machida, and O. Nilsson, *Phys. Rev. A* **34**, 4025 (1986); Y. Yamamoto and S. Machida, *ibid.* **35**, 5114 (1987).
 - ²S. Machida, Y. Yamamoto, and Y. Itaya, *Phys. Rev. Lett.* **58**, 1000 (1987).
 - ³P. R. Tapster, J. G. Rarity, and J. S. Satchell, *Europhys. Lett.* **4**, 293 (1987).
 - ⁴S. Machida and Y. Yamamoto, *Phys. Rev. Lett.* **60**, 792 (1988); W. H. Richardson, S. Machida, and Y. Yamamoto, *ibid.* **66**, 2867 (1991).
 - ⁵P. J. Edwards, *Int. J. Optoelectron.* **6**, 23 (1991).
 - ⁶J. Kim, H. Kan, and Y. Yamamoto, *Phys. Rev. B* **52**, 2008 (1995).
 - ⁷T. Hirano and T. Kuga, *IEEE J. Quantum Electron.* **QE-31**, 2236 (1995).
 - ⁸G. Shinozaki, T. Hirano, T. Kuga, and M. Yamanishi, *Jpn. J. Appl. Phys., Part 1* **36**, 6350 (1997).
 - ⁹J. Abe, G. Shinozaki, T. Hirano, T. Kuga, and M. Yamanishi, *J. Opt. Soc. Am. B* **14**, 1295 (1997).
 - ¹⁰M. Kobayashi, M. Kohno, Y. Kadoya, M. Yamanishi, J. Abe, and T. Hirano, *Appl. Phys. Lett.* **72**, 284 (1998).
 - ¹¹P. J. Edwards and G. H. Pollard, *Phys. Rev. Lett.* **69**, 1757 (1992).
 - ¹²H. Sumitomo, Y. Kadoya, and M. Yamanishi, *Opt. Lett.* **24**, 40 (1999).
 - ¹³G. Björk, *Phys. Rev. A* **45**, 8259 (1992).
 - ¹⁴E. Goobar, A. Karlsson, G. Björk, and P. J. Rigole, *Phys. Rev. Lett.* **70**, 437 (1993).
 - ¹⁵Y.-Q. Li, P. J. Edwards, P. Lynam, and W. N. Cheung, *Int. J. Optoelectron.* **10**, 417 (1995).
 - ¹⁶M. Yamanishi, K. Watanabe, N. Jikutani, and M. Ueda, *Phys. Rev. Lett.* **76**, 3432 (1996).
 - ¹⁷C. W. J. Beenakker and M. Büttiker, *Phys. Rev. B* **46**, 1889 (1992).
 - ¹⁸A. Shimizu and M. Ueda, *Phys. Rev. Lett.* **69**, 1403 (1992).
 - ¹⁹R. C. Liu and Y. Yamamoto, *Phys. Rev. B* **49**, 10 520 (1994).
 - ²⁰Y. Yamamoto and H. A. Haus, *Phys. Rev. A* **45**, 6596 (1992).
 - ²¹P. J. Edwards, *IEEE J. Quantum Electron.* **29**, 2302 (1993).
 - ²²J. Kim and Y. Yamamoto, *Phys. Rev. B* **55**, 9949 (1997).
 - ²³A. Imamoglu, Y. Yamamoto, and P. Solomon, *Phys. Rev. B* **46**, 9555 (1992); A. Imamoglu and Y. Yamamoto, *ibid.* **46**, 15 982 (1992).
 - ²⁴A. Imamoglu and Y. Yamamoto, *Phys. Rev. Lett.* **70**, 3327 (1993).
 - ²⁵K. Kurata, Y. Ono, K. Ito, M. Mori, and H. Sano, *IEEE Trans. Electron Devices* **ED-28**, 374 (1981).
 - ²⁶M. Yamanishi and Y. Lee, *Phys. Rev. A* **48**, R2534 (1993).
 - ²⁷For instance, H. C. Casey, Jr. and M. B. Panish, *Heterostructure Lasers* (Academic Press, New York, 1978), Pt. A, Chap. 3, p. 161.
 - ²⁸For instance, J. Shah, *Solid-State Electron.* **21**, 43 (1978).
 - ²⁹For instance, H. Kressel and J. K. Butler, *Semiconductor Lasers and Heterojunction LEDs* (Academic Press, New York, 1977), Chap. 2, p. 56.
 - ³⁰S. Zukotynski, S. Sumski, M. B. Panish, and H. C. Casey, Jr., *J. Appl. Phys.* **50**, 5795 (1979).
 - ³¹*Hitachi Optodevice Data Book* (Hitachi Co., Tokyo, 1996) (in Japanese).
 - ³²In Ref. 25, the internal series resistance at room temperature of the same type LED as ours was assigned to be, for instance, 1.3Ω for the acceptor concentration, $N_a = 4 \times 10^{18} \text{ cm}^{-3}$, and the thickness $t = 30 \mu\text{m}$ of the p -type wide-band-gap layer. However, in the reference, the resistances were fitted by an empirical design curve, $R_s \propto 1/(N_a^{2.8} t^{6.5})$, which is quite unphysical. The resistance should, in general, be inversely proportional to N_a and t . Probably, different growth conditions used to obtain different N_a and t values lead to different n -side barrier heights ϕ_n through different grading layer thicknesses and, in turn, different BP rates (see Appendix B).
 - ³³H. Sumitomo, Y. Kadoya, and M. Yamanishi (unpublished).
 - ³⁴M. Kobayashi, Y. Kadoya, H. Yuji, R. Masuyama, and M. Yamanishi (unpublished).
 - ³⁵For instance, W. W. Chow, S. W. Koch, and M. Sargent III, *Semiconductor-Laser Physics* (Springer-Verlag, Berlin, 1994), Chap. 9, pp. 345–348.
 - ³⁶D. T. Cheung, S. Y. Chiang, and G. L. Pearson, *Solid-State Electron.* **18**, 263 (1975).
 - ³⁷See for instance, H. C. Casey, Jr. and M. B. Panish, *Heterostructure Lasers* (Ref. 27), Chap. 4, p. 193.
 - ³⁸H. Kroemer, *Surf. Sci.* **174**, 299 (1986).
 - ³⁹See for instance, H. C. Casey, Jr. and M. B. Panish, *Heterostructure Lasers* (Ref. 27), Chap. 4, pp. 231–235.